Plasma-assisted ammonia synthesis in a packed-bed dielectric barrier discharge reactor: effect of argon addition

Jin Liu[1], Xinbo Zhu[1, *], Xueli Hu[1, 3], Fei Zhang[1], Xin Tu[2, *]

[1]Faculty of Maritime and Transportation, Ningbo University, Ningbo 315211, China

[2]Department of Electrical Engineering and Electronics, University of Liverpool, Liverpool L69 3GJ, United Kingdom

[3]SAIC Volkswagen Automotive Co., Ltd., Ningbo 315460, China

Abstract

The effect of argon (Ar) addition on plasma-assisted ammonia (NH_3) synthesis in a packed-bed dielectric barrier discharge (DBD) reactor is investigated in this work. Both higher normalized NH_3 concentration and N_2 conversion are achieved by adding Ar to N_2–H_2 plasma. The 18.6% increment of normalized NH_3 concentration and 15% increment of N_2 conversion are realized with 30 vol.% Ar addition compared with the case of N_2–H_2 plasma only, indicating that Ar addition would contribute to NH_3 formation. The mechanisms of NH_3 synthesis with Ar addition are proposed based on electrical characteristics and electron energy distribution function of the N_2–H_2–Ar plasma. The intensity of microdischarges, mean electron energy and quantity of energetic electrons increase upon Ar addition. Hence, the electron-impact reactions would be enhanced upon Ar addition. Meanwhile, the effective capacitance of the plasma reactor is improved, which suggests Ar addition contributes to achieve fully-bridged plasma discharge and transfer energy into chemical process in plasma. Moreover, the presence of Ar generates Penning excitation and ionization reactions, which would benefit N_2 conversion and then accelerate NH_3 formation as well.

Keywords: plasma, dielectric barrier discharge, ammonia synthesis, Ar addition, optical emission

spectrum

1. Introduction

Ammonia (NH_3) is the second largest chemical products in the world and one of the most common precursors to manufacture many useful products including plastic, polyester fiber, fertilizer and medicine[1–3]. Recently, ammonia has attracted extensive attention to be used as a clean fuel[4–6]. The use of NH_3 in combustion processes, such as internal combustion engines, gas turbines and firepower electricity production as the alternative of fossil fuels, can be a promising solution in reduction of carbon emission[7–9].

Conventional industrial-scale NH_3 synthesis method is Haber-Bosch (HB) method. However, the HB method requires harsh reaction conditions, *e.g.* sustained high temperature (500–600°C) and high pressure (20–40 MPa). As a result, the HB method consumes ultra-large amount of energy (1%–2% of world's primary energy supply)[10]. In the past few decades, several alternative methods have been used in NH_3 synthesis as the substitutes of HB method, including biochemical process, electro-chemical process and non-thermal plasma (NTP) assisted process. Among these methods, NTP assisted method is particularly promising to alternate the conventional HB method due to the mild operation conditions and good economy. The NTP is contributed to the generation of highly reactive species and breaking the limits of thermodynamics[11]. A variety of NTPs have been investigated for NH_3 synthesis, including dielectric barrier discharge (DBD)[12, 13], radio frequency discharge[14, 15] and glow discharge[16] plasmas. Among them, the DBD plasma is particularly applicable due to its feasibility to integrate with catalysts or dilution gases.

It has been recognized that the addition of dilution gas could affect the electrical

characteristics of plasma, while the electrical characteristics could accelerate the reaction kinetics in turn. For example, Ramakers *et al.* studied the effect of argon or helium addition on the electrical parameters in plasma-assisted CO_2 conversion. The 95% Ar addition reduced the breakdown voltage to 1.05 kV, while the breakdown voltage is 2.06 kV for pure CO_2 plasma. The lower breakdown voltage suggested that a larger fraction of applied power can be used effectively for CO_2 conversion. As the result, when the Ar content increased from 0 vol.% to 50 vol.%, the CO_2 conversion increased by 80%[17]. Moss *et al.* reported the effects of Ar addition on CO_2 conversion and reported that the addition of Ar produced a substantial increment in rate constants of CO_2 dissociation via electron impact. At the SIE of 0.2 eV/molecule, compared with pure CO_2 plasma, the energy efficiency was 1.25-fold higher upon 50 vol.% Ar addition[18]. Chen *et al.* reported that the addition of Ar into O_2 plasma would lead to a higher discharge power at a fixed applied voltage. For instance, compared to that without Ar addition, 2 times improvement in plasma discharge power was achieved once 50 vol.% Ar was added, while the O_3 concentration was 14.05% higher when V_{pk} is 15 kV[19].

Recently, some researchers have recognized that the employment of dilution gas could improve the conversion of reactants towards targeted products. Zeng *et al.* investigated the effect of argon addition on plasma-catalytic hydrogenation of CO_2 for the co-generation of CO and CH_4. It was reported that the addition of Ar in the feed gas enhanced the conversion of CO_2 and the production efficiency. For instance, raising the Ar content from 0 vol.% to 60 vol.% significantly reduced the CO/CH_4 molar ratio from 24 to 12[11]. Kholodkova *et al.* researched the effect of Ar addition on the dissociation of oxygen molecules. The results indicated that an increase in the inert gas content in plasma caused a monotonic growth of the degree of dissociation of oxygen molecules, while the overall rate of production of oxygen atoms at an oxygen content of over 50 vol.% remained

constant[20]. However, many challenges still remain for revealing the mechanisms of interaction between reactants and plasma.

In this work, the effects of Ar as a dilution gas on the plasma-assisted NH_3 synthesis have investigated in terms of NH_3 concentration and N_2 conversion. The mechanisms of effect of Ar addition on NH_3 synthesis are explained by studying electrical characterization of the plasma, optical emission spectra plasma and electron energy distribution function (EEDF) calculated by BOLSIG+.

2. Experimental setup

2.1. Experimental system

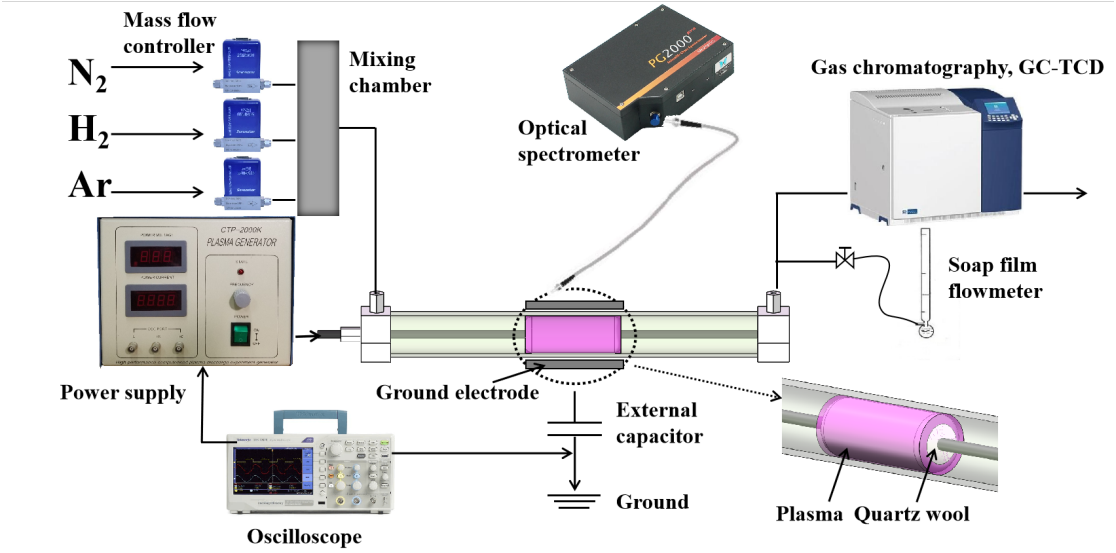

Fig. 1 Experimental setup for the plasma-assisted synthesis of NH_3

Fig. 1 is the schematic diagram of the experimental system setup. The reactor was a coaxial packed-bed DBD reactor. A quartz tube with the inner diameter of 8 mm and the thickness of 2 mm was used as the dielectric barrier. The reactor was packed with quartz wool, while the length of the packed region was kept at 40 mm. A stainless rod with the diameter of 4 mm was used as the high

voltage electrode and connected with the power supply (Suman CTP2000K). Stainless steel mesh with the length of 40 mm was wrapped around the quartz tube and served as the outer electrode. An external capacitor (C_{ext} = 0.47 μF) was connected between the outer electrode and ground. The voltage across the external capacitor was measured to obtain the quantity of transferred charges (Q_{trans}) during the plasma discharge process. Both the voltage across the external capacitor and the applied voltage across the reactor were measured by high voltage probes (Tektronix TPP0502). All electrical signals were sampled by a four-channel digital oscilloscope (Tektronix TDS2024C). The discharge power was obtained by calculation of areas of the *Q-U* Lissajous figure.

Zero grade (purity > 99.999%) N_2, H_2 and Ar were provided from gas cylinders and regulated by mass flow controllers (Sevenstars D07-B). Before being introduced to the reactor, the gas streams were mixed in a mixing chamber. The gas products were analyzed by two-channel gas chromatography (Fuli 9790II), which was equipped with a thermal conductivity detector (TCD). The gas concentration was measured 5 times and given average value. The optimal emission spectrum was measured using a spectrometer (Ideaoptics PG2000-PRO-EX). Electron energy loss fraction and mean electron energy were calculated by BOLSIG+[21].

2.2. Parameters calculation

An equivalent circuit developed from our previous work is used to simplify and describe the pack-bed DBD reactor in this work[11]. The reactor is considered to be composed by four capacitors as shown in Fig. 2.

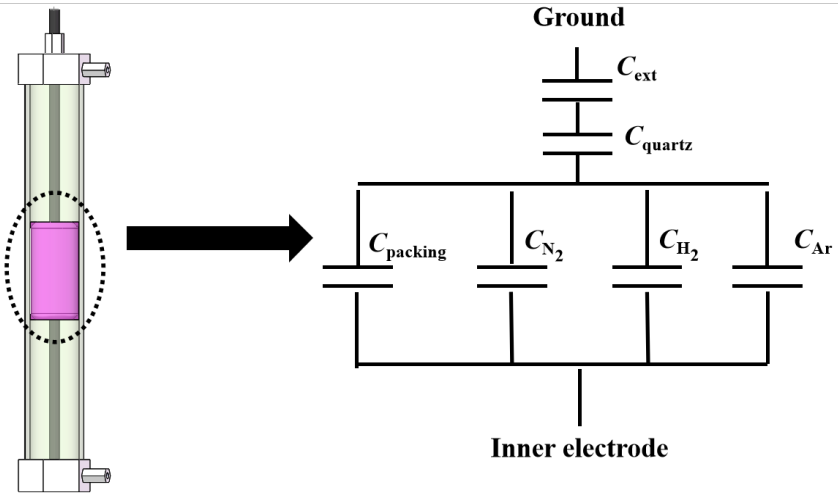

Fig. 2. Equivalent circuit diagram for the discharge zone of reactor

The capacitance of the reactor in plasma-off phase (C_{total}) could be calculated by following equation:

$$\frac{1}{C_{total}} = \frac{1}{C_{quatrz}} + \frac{1}{C_{gap}} = \frac{1}{C_{quartz}} + \frac{1}{C_{N_2} + C_{H_2} + C_{Ar} + C_{packing}} \quad (1)$$

where C_{quarz} is the capacitance of quartz tube. C_{N_2}, C_{H_2}, C_{Ar} and $C_{packing}$ are the capacitances of nitrogen, hydrogen, argon and the packing materials, respectively.

The total capacitance of the reactor (C_{cell}), effective capacitance of (C_{eff}), peak-to-peak voltage (U_{pk}), quantity of transferred charges (Q_{trans}), quantity of discharged charges (Q_{dis}) and the minimum voltage at the beginning of charge transferring (U_{min}) of the plasma discharge process could be obtained from the Lissajous figure (as shown in Fig. 3).

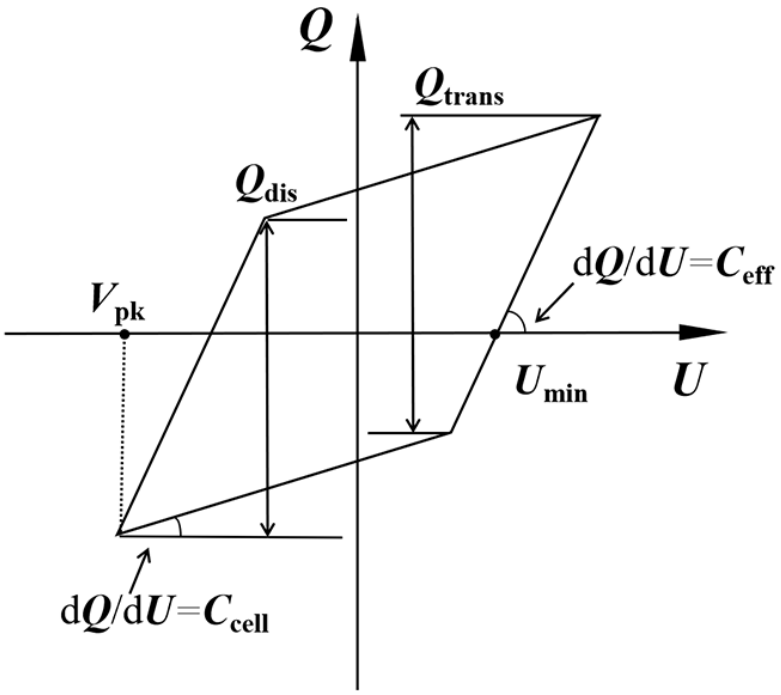

Fig. 3. Schematic figure for the derivation of electrical parameters from the *Q–U* Lissajous

The discharge power based on the Lissajous method could be calculated by [22]:

$$P_{\mathrm{dis}}(\mathrm{W}) = f(\mathrm{Hz}) \times C_{\mathrm{ext}}(\mu\mathrm{F}) \times A \tag{2}$$

where C_{ext} is external capacitance (0.47 μF), f is the frequency of AC discharge. In this work, the frequency of AC discharge was kept in the range of 9.2 to 9.8 kHz. A is the area of the Lissajous figures.

The specific input energy (SIE) of the plasma-assisted process is as follow:

$$SIE(\mathrm{kJ \cdot L^{-1}}) = \frac{60 \times P_{\mathrm{dis}}(\mathrm{kW})}{Q(\mathrm{L \cdot min^{-1}})} \tag{3}$$

where Q denotes total flow rate and is fixed at 0.1 $\mathrm{L \cdot min^{-1}}$.

The voltage applied on the gap of the reactor can be calculated as follow:

$$U_{\mathrm{gap}}(\mathrm{kV}) = U_{\mathrm{app}} - U_{\mathrm{quartz}} = U_{\mathrm{app}} - \frac{C_{\mathrm{ext}}(\mathrm{pF}) \times U_{\mathrm{ext}}(\mathrm{kV})}{C_{\mathrm{quartz}}(\mathrm{pF})} \tag{4}$$

where U_{gap} is the voltage across the gap of the reactor, U_{app} is the applied voltage, U_{quartz} is the

voltage applied on quartz tube and U_{ext} is the voltage across the external capacitance.

The following equations are used to calculated C_{gas} and U_b:

$$C_{gas}(\mathrm{pF}) = \frac{C_{eff}(\mathrm{pF}) \times C_{total}(\mathrm{pF})}{C_{eff}(\mathrm{pF}) - C_{total}(\mathrm{pF})} \tag{5}$$

where C_{gas} is the actual capacitance of the gas mixtures.

$$U_b(\mathrm{kV}) = \frac{U_{min}(\mathrm{kV})}{1 + \frac{C_g(\mathrm{pF})}{C_{eff}(\mathrm{pF})}} \tag{6}$$

where U_b is the breakdown voltage of the DBD reactor.

The reduced electric field strength (E/N) is calculated by:

$$E/N(\mathrm{Td}) = \frac{U_b(\mathrm{kV}) \times 10^{-24}}{N \times d_g(\mathrm{m})} \tag{7}$$

where N is the number density of gas molecules, which is approximately 2.4×10^{25} m^3 at atmosphere pressure and temperature. d_g is the equivalent gap thicknesses of gas phase in the packed region.

The N_2 conversion rate is defined as follows:

$$X_{N_2}(\%) = \frac{C_{NH_3}(\mathrm{ppm})}{2 \times C_{N_2}(\mathrm{ppm})} \tag{8}$$

where C_{NH_3} is the outlet concentration of NH_3, C_{N_2} is the input concentration of N_2.

The electron energy loss fraction is defined as follow:

$$E_{loss}(\%) = \frac{E_i(\mathrm{eV})}{E_{total}(\mathrm{eV})} \tag{9}$$

where E_{total} is the energy of electrons, E_i (i could be excitation or ionization) is the electron energy spent on the excitation or ionization of the feed gases.

The normalized NH_3 concentration (C_{norm}) is as follow[23]:

$$C_{\text{norm}} = \frac{C_{\text{NH}_3}(\text{ppm})}{r_{(\text{H}_2+\text{N}_2)}(\%)} \tag{10}$$

where $r_{(H_2+N_2)}$ denotes the total proportion of N_2 and H_2 in feed gases.

3. Results and discussions

3.1. Effect of Ar addition on electrical characteristics

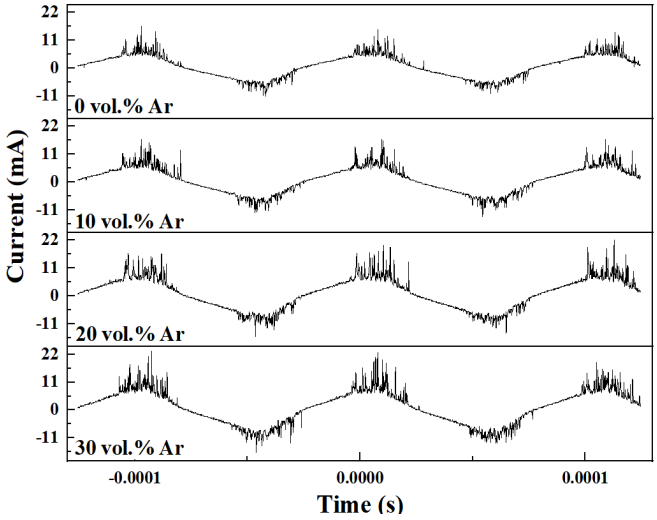

Fig. 4. Effect of Ar addition on current profiles at the SIE of 15 kJ·L^{-1}.

Fig. 4 illustrates the current profiles for N_2–H_2–Ar plasma with different Ar content. It is visible that the current waveform is the sinusoidal waveform. Numerous spikes are presented in the current peaks every half-period, indicating the presence of microdischarges. The higher spikes suggest the intensified filimentary discharges or superposition of several microdischarges occurring simultaneously[24]. The amplitude of sinusoidal current, as well as the intensity of filamentary microdischarges, is significantly higher with Ar addition. When the Ar content is 30 vol.%, the time-averaged intensity of the microdischarges in the positive period of the current waveform is 11.88 mA at the peak of positive half-period, which is 7.22% and 37.49% higher than the cases of 20 vol.% and 0 vol.% Ar addition, respectively. It could be inferred that a larger fraction of charges is transferred into the plasma upon Ar addition, as could also be deduced from the Lissajous figures.

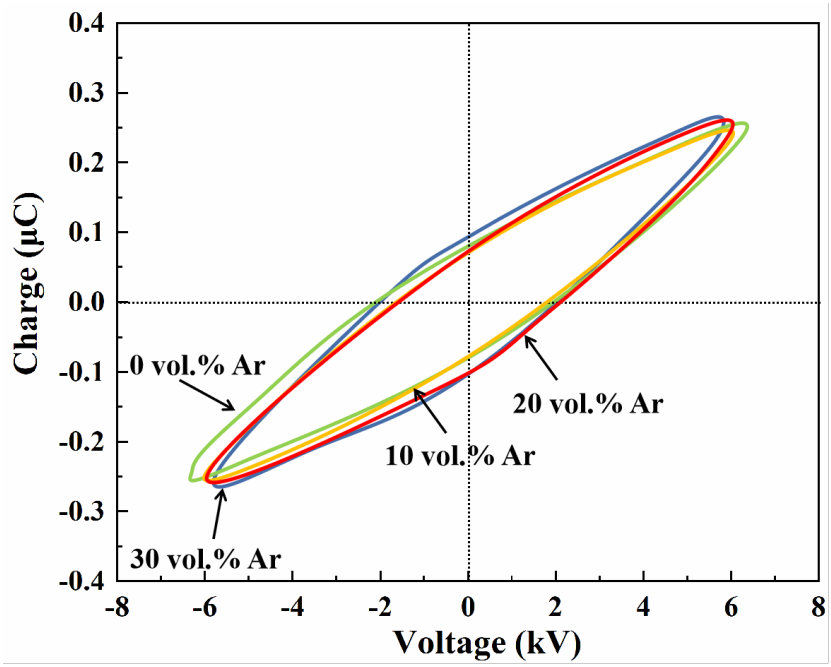

Fig. 5. Lissajous figures for DBD reactors with different Ar content (SIE = 15 kJ·L^{-1}, gas flow rate = 100 mL·min^{-1}, N_2/H_2 = 1:1)

Table 1. Electrical parameters of plasma upon Ar addition, as deduced from the Lissajous figures in figure 5.

Content	Q_{trans} (μC)	C_{eff} (pF)	C_{total} (pF)	U_b (kV)
0 vol.% Ar	0.29	90.91	47.11	1.06
10 vol.% Ar	0.30	96.36	49.31	0.98
20 vol.% Ar	0.33	103.66	45.16	0.92
30 vol.% Ar	0.34	117.65	44.91	0.84

Fig. 5 shows the Lissajous figures of the reactor with different Ar content at the SIE of 15 kJ·L^{-1}. The electrical parameters of plasma upon Ar addition are listed in Table 1. The shape of the Lissajous figure changes upon Ar addition, which suggests the changes in the electrical characteristics of plasma including C_{total}, C_{eff}, and Q_{trans}. The Q_{trans} is 0.34 μC when 30 vol.% Ar is added, which is 17.24% higher than that without Ar addition. Similar phenomenon was reported by Li *et al.* that both the intensity of the microdischarges, as well as the amount of transferred charges are significantly higher than in the case of Ar–CO_2 mixtures[25]. In addition, the breakdown voltage decreases from 1.06 kV to 0.84 kV upon 30 vol.% Ar addition. This is in good agreement with other works[11, 17] and could be explained that the average electric field strength is increased when Ar

accounts for a larger proportion of the mixed gases[26].

Ideally, the C_{eff} equals to the capacitance of the dielectric barrier when the discharge gap is fully bridged by plasma[27]. However, we find that the C_{eff} value is lower than the capacitance of quartz tube in this work. This phenomenon might be caused by the nonuniform formation of the microdischarges in the plasma region[28]. A similar observation was reported by Zhang *et al.* that a homogeneous diffuse plasma with a larger area was generated by adding Ar to N_2 plasma[29]. In this case, many charges could not be transferred into the plasma and would cause a waste of energy. A larger effective capacitance of 44.39 pF is achieved upon 30 vol.% Ar addition, which is 16.89% higher than the case without Ar addition. The higher C_{eff} suggests the addition of Ar is found to bridge the gap between the electrodes and enhance the charge transfer between them[11].

3.2. Effect of Ar addition on electron energy

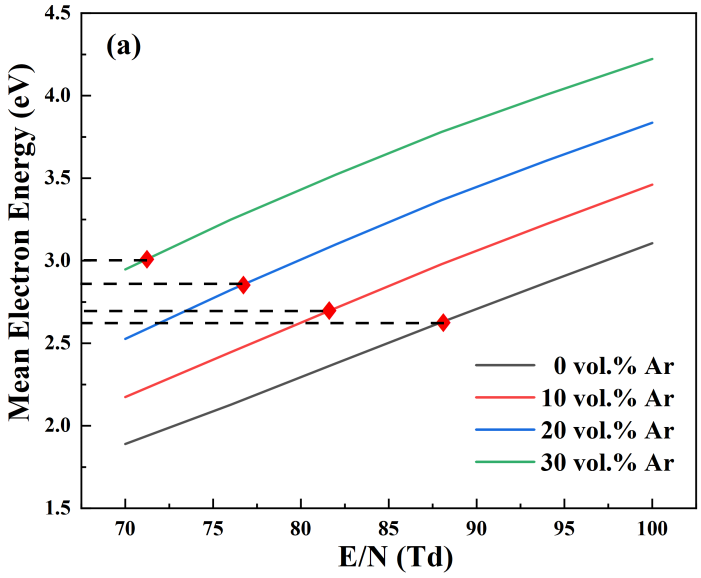

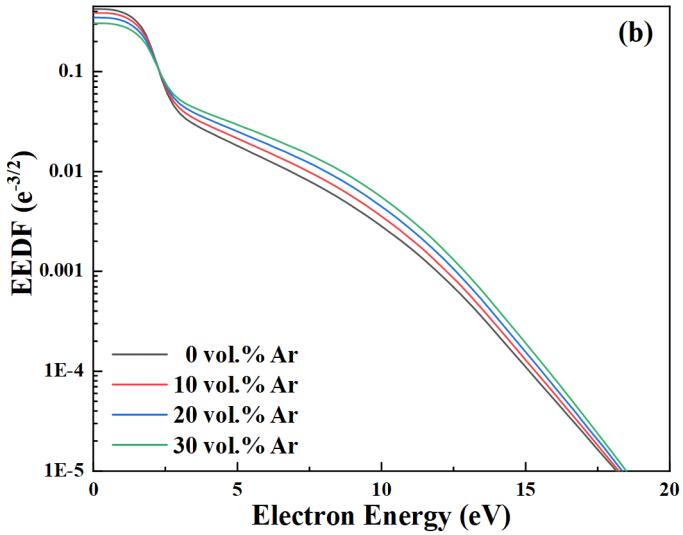

Fig. 6. Effect of Ar content on electrical parameters of plasma (a) mean electron energy; (b) EEDF (SIE = 15 kJ·L^{-1}, gas flow rate = 100 mL·min^{-1}, N_2/H_2 = 1:1)

The mean electron energy and EEDF for the cases with different Ar content are presented in Fig. 6. The red points in Fig. 6(a) correspond to the mean electron energy for the cases with different content at the same SIE of 15 kJ·L^{-1}. It is obvious that with the increasing content of Ar, the mean electron energy is improving, which corresponds to the higher average electric field. Particularly, since the Ar content increases in the range of 0 vol.% to 30 vol.%, the mean electron energy grows from 2.62 eV to 3.02 eV. This phenomenon could be explained by the lower probability of the electrons for inelastic collisions with Ar and for recombination with Ar ions, which results in a longer mean free path of the electrons upon Ar addition. Hence, the electrons could be further accelerated at the same *E/N*[17]. Fig. 6(b) presents the EEDF for the cases upon different Ar content corresponding to the red points in Fig. 6(a). Although the *E/N* is decreasing following the increase of Ar content in feed gases, the electron energy distribution function shift with an increase in electron density in the high-energy tail of the distribution function, indicating the fraction of the electrons with higher energy is increasing with higher Ar content[30]. In the plasma, electrons would transfer their energy to gas molecules via the electron-impact reactions, mainly including rotational and vibrational, and electronic excitation with lower energy states[19]. Hence, with the increasing

Ar content, more chemically reactive species can be generated in the plasma region via electron impacts to drive the plasma chemical reactions.

3.3. OES for N_2–H_2–Ar plasma

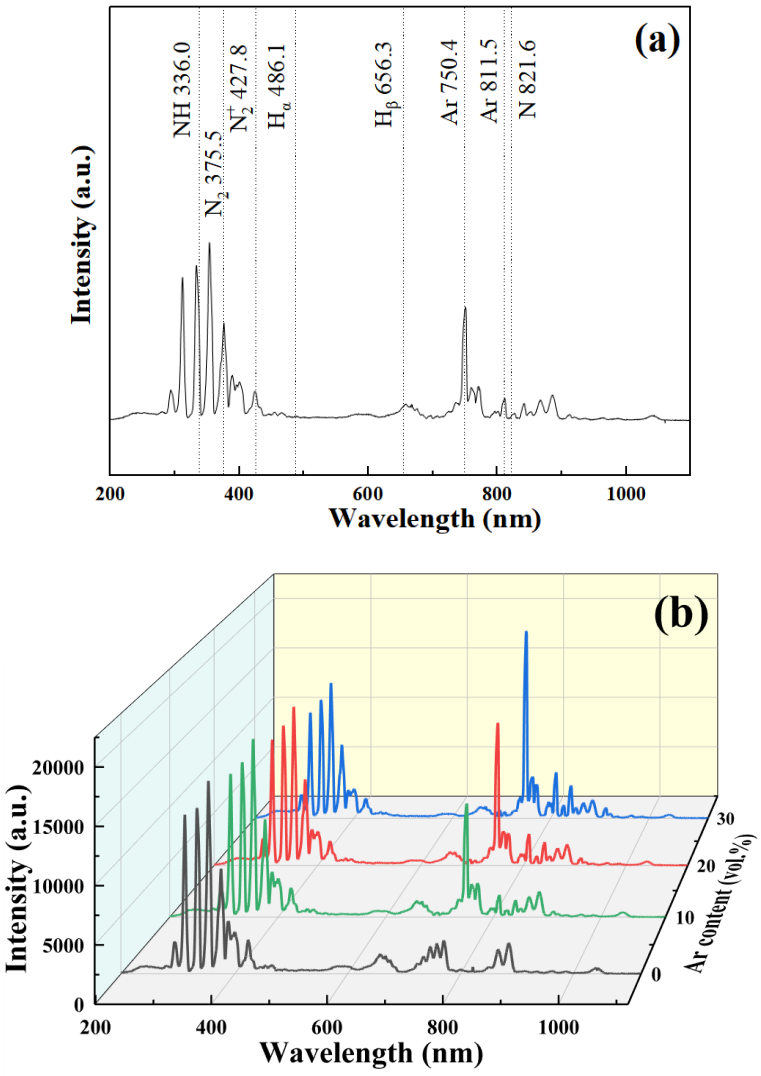

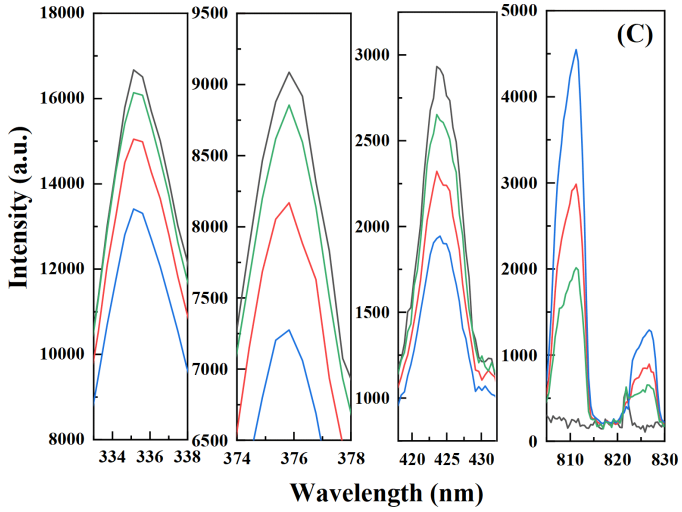

Fig. 7. Optical emission spectra for N_2–H_2–Ar plasma with different Ar content (a) typical spectrum for N_2–H_2–Ar plasma in theory; (b) and (c) effect of Ar content on plasma spectra (SIE = 15 kJ·L^{-1}, gas flow rate = 100 mL·min^{-1}, and gas feed ratio is 1:1. Black, green, red and blue lines are for the cases of 0, 10, 20 and 30 vol.% Ar contents, respectively.)

Fig. 7 is the optical emission spectra (OES) for N_2–H_2–Ar plasma, recorded at the SIE of 15 kJ·L^{-1}. Fig. 7(a) presents the theoretically spectrum for N_2–H_2–Ar plasma. Line assignments with identified spectral features are obtained from literature values of the spectroscopic constants[31–37]. The intensity of characteristic spectrum lines presents relative concentrations of the corresponding species. Fig. 7(b) and 7(c) presents the spectra for N_2–H_2–Ar plasma with different Ar content in this work. The main features of the spectra are the second positive system (SPS) N_2 ($C^3\Pi_u \rightarrow B^3\Pi_g$), the first positive system (FPS) N_2 ($B^3\Pi_u \rightarrow A^3\sum_g$), the first negative system (FNS) N_2^+ ($B^2\sum_u^+ \rightarrow X^2\Pi_g^+$) and Ar I band. The peaks within the wavelength ranging from 292 nm to 428 nm mainly belong to the FPS and SNS system of N_2. This phenomenon indicates that N_2 have been excited (N_2^*) and ionized (N_2^+). The presence of Ar atomic lines (at 750.4 and 811.5 nm) suggests the excitation of Ar and the generation of Ar* ($^3P_2$,$^3P_0$). With the increasing content of Ar, the intensity of Ar (811.5 nm) line is increasing. This phenomenon indicates more Ar atoms are excited by electron-impact. Theoretically, the concentration of H active species could be determined by the intensities of H_α and H_β characteristic lines. However, these lines are hardly noticeable or partially

overlapped by the Ar lines in this work. As far as we know, there is no previous work in which emission from atomic H was clearly detected in packed-bed DBD reactor under the similar operation conditions and gas composition. Similar phenomena were also reported by Miotk *et al.*[38], and Gomez-Ramirez *et al.*[39].

The NH· band head at 336 nm could also be identified as a shoulder peak at a N_2 characteristic peak. It has been proved that the NH· radical is mainly generated from the combination of N· and H· (R1)[39, 40]. Therefore, identification of NH characteristic peak not only suggests the generation of NH·, but also the generation of H·. On the other hand, the dissociation energy for N_2 is much higher than that for H_2. The identification of N atomic line suggests the dissociation of N_2, which also indicates the generation of H· would happen in the plasma theoretically.

$$N\cdot + H\cdot \rightarrow NH\cdot \qquad \text{(R1)}$$

3.4. Effect of Ar addition on N_2 conversion and NH_3 formation

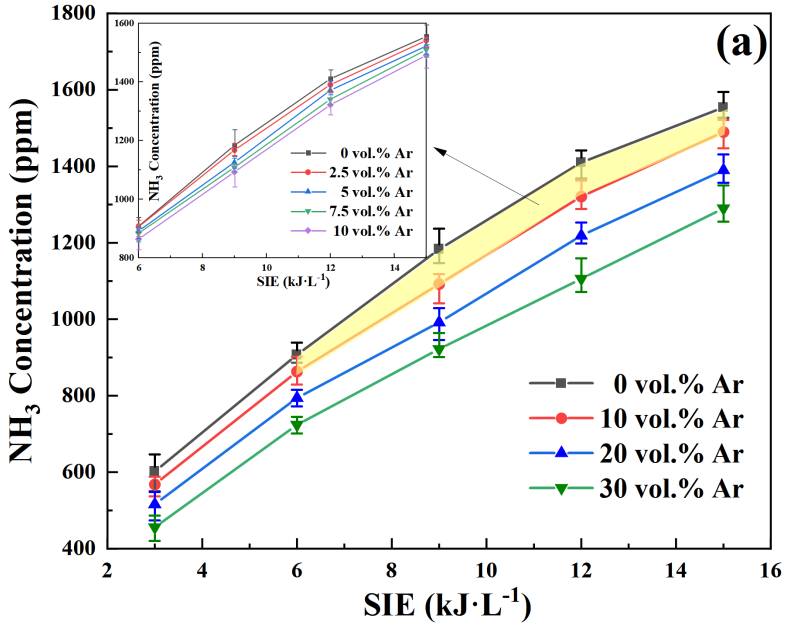

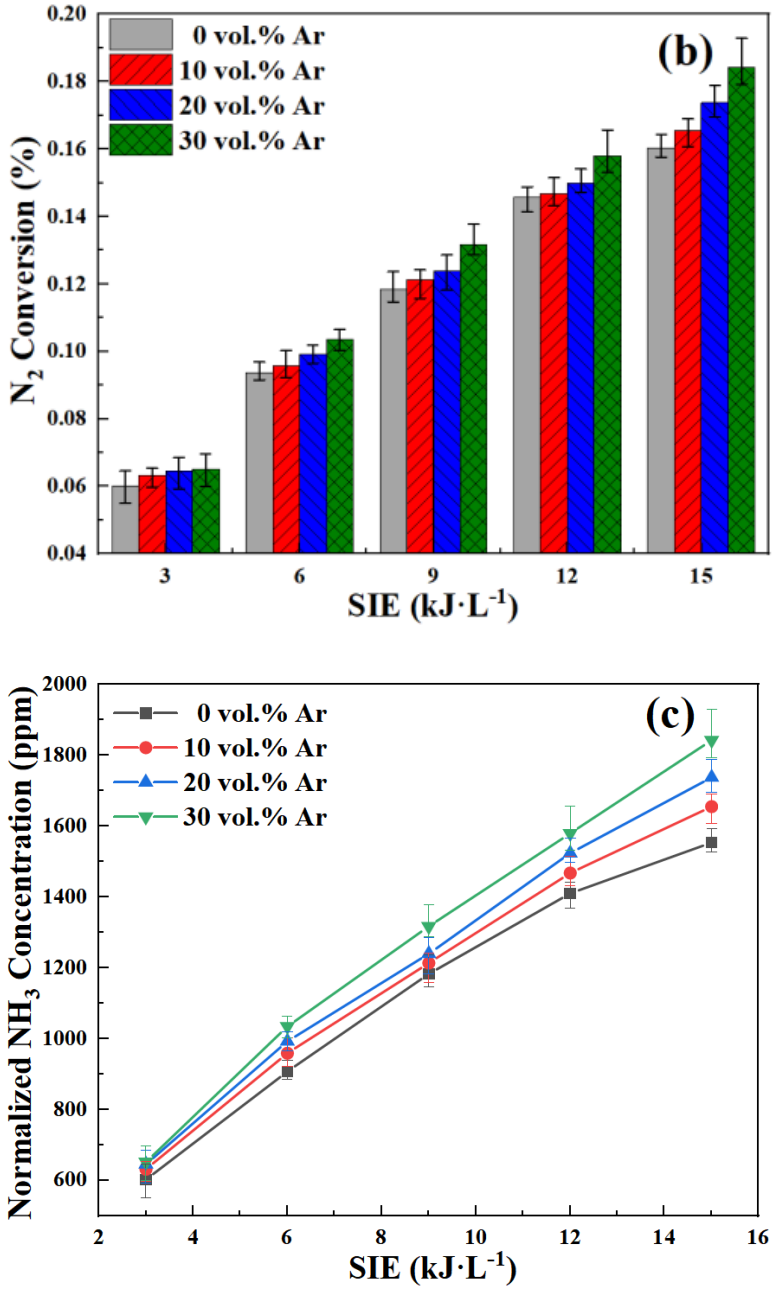

Fig. 8. Effect of Ar addition on (a) NH_3 concentration; (b) N_2 conversion; and (c) normalized NH_3 concentration

Fig. 8(a) presents the effect of Ar addition on NH_3 concentration at different SIE. When the SIE increases from 3 kJ·L^{-1} to 15 kJ·L^{-1}, the NH_3 concentration increases in the range of 602 ppm to 1604 ppm without Ar addition. Compared at the SIE of 15 kJ·L^{-1}, the NH_3 concentration only decreases by 4.13% while the gas mixture is diluted by 10 vol.% Ar. Clearly, NH_3 concentration decreases upon Ar addition, which could be attributed to the dilution of formed NH_3 by Ar[24]. Fig.

8(b) depicts the conversion of N_2 upon Ar addition. At a fixed SIE, the N_2 conversion increases with the increasing Ar content. For example, at the SIE of 15 kJ·L^{-1}, the highest N_2 conversion is 0.18% with 30 vol.% Ar addition, which is 18.79% higher than that without Ar addition. This phenomenon suggests that N_2 could be easily transformed upon Ar addition. Hence, it can be concluded that a higher Ar content would promote NH_3 formation, which can be further elucidated by Fig. 8(c).

Fig. 8(c) presents the normalized NH_3 concentration with different Ar content. At a fixed SIE, the C_{norm} is increasing monotonically following the increasing Ar content. The highest C_{norm} is achieved at the SIE of 15 kJ·L^{-1} with 30 vol.% Ar content, which is 18.62% higher than that of pure N_2–H_2 plasma. The increasing value of C_{norm} indicates more NH_3 is generated per unit volume of N_2 and H_2 by adding Ar to the feed gas. One of the reasons is that the addition of Ar could firstly affect the electrical characteristics of plasma, while these electrical characteristics would in turn affect electron-impact reactions, the initial steps of plasma chemistry. As described in section 3.1, both higher C_{eff} and Q_{trans} are obtained upon Ar addition, indicating that more energy could be injected into the plasma for chemical reactions, as less power would be dissipated for gas breakdown[11, 41]. Meanwhile, the addition of Ar leads to the improvement in both mean electron energy and the quantity of energetic electrons as well. As the result, the generation of various neutral and charged products as given in R2–R5, including excited species like N_2^*, H_2^*, N·, H· radicals and ions, would be accelerated upon Ar addition. In the plasma, for electron with low energies, the highest reaction rates are expected for elastic scattering and vibrational excitation since these reactions show the largest collisional cross sections[42]. Therefore, the concentration of molecules in excitation state, *e.g.* N_2^* and H_2^*, is considered to be much higher. These species could be easily dissociated (*i.e.* R3) then combine with each other, contributing the formation of NH_x (x = 1 or 2)

as the intermediates and consequently NH_3 molecules (*i.e.* R6)[40, 43, 44]. The EEDF for electron with high energy is considerably smaller, suggesting that the rate constants for electron-impact ionization reactions (generating N_2^+ and H_2^+, R4) are orders of magnitude smaller than electron-impact excitation reactions[45]. These charged molecules would be involved in ion-molecule reactions, yielding H· radical and N_2H^+ ions (R5)[46].

$$N_2 \text{ or } H_2 + e \rightarrow N_2^* \text{ or } H_2^* + e \quad \text{(R2)}$$

$$N_2^* \text{ or } H_2^* + e \rightarrow 2N\cdot \text{ or } 2H\cdot + e \quad \text{(R3)}$$

$$N_2 \text{ or } H_2 + e \rightarrow N_2^+ \text{ or } H_2^+ + e \quad \text{(R4)}$$

$$N_2 \text{ or } H_2 + N_2^+ \rightarrow N_2H^+ + H\cdot \quad \text{(R5)}$$

$$N\cdot + xH\cdot \rightarrow NH_x \xrightarrow{+H} NH_3 \quad \text{(R6)}$$

Except for the enhancement in electron-impact reactions, it is worth to mention that in the N_2–H_2–Ar mixtures, Penning excitation and ionization reactions would be responsible for the enhancement in N_2 dissociation and consequently NH_3 formation as well. As proved in the previous section, a portion of the energy is transferred from the electrons to the excitation/ionization modes of the Ar. Previous study reported that once the argon atom is energized, the stored energy of Ar^* or Ar^+ could be utilized to Penning excitation and dissociation reactions (*e.g.* R7–R9)[46]. Furthermore, there would exist charge transfer of the Ar^+ ions with N_2 and H_2, yielding N_2^+, H_2^+ and H_3^+ ions (*i.e.* R10 and R11)[47, 48]. These Penning reactions would also contribute to the generation of chemically active species, which would further accelerate the formation of immediate species and consequently NH_3 molecules.

$$N_2 \text{ or } H_2 + Ar^* \rightarrow N_2^* \text{ or } H_2^* + Ar \quad \text{(R7)}$$

$$N_2 \text{ or } H_2 + Ar^* \rightarrow 2N\cdot \text{ or } 2H\cdot + Ar \quad \text{(R8)}$$

$$N_2 \text{ or } H_2 + Ar^+ \rightarrow 2N\cdot \text{ or } 2H\cdot + Ar^+ \quad \text{(R9)}$$

$$N_2 \text{ or } H_2 + Ar^+ \rightarrow N_2^+ \text{ or } H_2^+ + Ar \quad \text{(R10)}$$

$$2H_2 + Ar^+ \rightarrow H_3^+ + H\cdot + Ar \quad \text{(R11)}$$

As shown in Fig. 8, compared with the case of 0 vol.% Ar addition, the intensity of N atomic line keeps increasing even the N_2 concentration is diluted by 10 vol.% Ar addition. It has been proved that N atoms are mainly generated from the dissociation of N_2^+ in plasma[40, 48]. By combining the information obtained from Fig. 7 and 8, the increasing intensity of N atomic line suggests N_2 excitation-ionization reactions are enhanced upon Ar addition. Therefore, compared with that of N_2–H_2 plasma, the N_2 conversion is improved by 4.53% to 8.13% upon Ar addition. Similar phenomenon was also reported by Li *et al.* that with 87% Ar dilution, the conversion of N_2 increased more than five times with 1.5 times increase in energy consumption comparing with no dilution condition[25]. The higher concentration of N· species could promote the formation of NH_x species (*i.e.* R6)[35]. In this work, upon 10 vol.% Ar addition, the intensity of NH line slightly decreases by 3.71%, which could be attributed to that the NH· species generates initially and then diluted by the Ar. The generation of NH· radical, which is the important intermediate of NH_3 formation, could accelerate NH_3 formation in gas phase[40, 49]. As the result, with the Ar content increases from 10 vol.% to 30 vol.%, the C_{norm} increase by 6.22% to 18.62% compared with that of N_2–H_2 plasma, which suggests that by utilizing the beneficial effect of argon addition, much higher yields of ammonia could be achieved.

4. Conclusions

Plasma-assisted NH_3 synthesis has been carried out in a packed-bed DBD reactor upon Ar

addition. The effect of the Ar addition on NH_3 concentration has been investigated in terms of normalized NH_3 concentration and N_2 conversion. Both normalized NH_3 concentration and N_2 conversion are monotonically increasing with the increasing Ar content, which suggests Ar addition is beneficial for NH_3 formation. At the SIE of 15 $kJ \cdot L^{-1}$, the normalized NH_3 concentration is 1824 ppm with 30 vol.% Ar addition, which is 18.62% higher than that of N_2–H_2 plasma only. Compared with the case of N_2–H_2 plasma only, the N_2 conversion is improved by 4.53% to 8.13% upon Ar addition.

The mechanisms of effect of Ar addition on plasma-assisted NH_3 synthesis are illustrated. The electron-impact reactions are enhanced due to the increase number of energetic electrons, quantity of transferred charges, and the discharge power injected into plasma upon Ar addition. It is worth to mention that besides of enhancement in electron-impact reactions, Penning excitation and ionization reactions would also be responsible for the conversion of feed gases and consequently NH_3 formation when Ar is added in gas mixtures. All these effects can explain the higher normalized NH_3 concentration achieved upon Ar addition.

Acknowledgments

The authors are grateful for the financial support from National Natural Science Foundation of China (No.51976093) and K.C. Wong Magna Fund in Ningbo University.

References

[1] A. Valera-Medina, H. Xiao, M. Owen-Jones, W.I.F. David, P.J. Bowen, Ammonia for power, Progress in Energy and Combustion Science 69 (2018) 63–102.
[2] C. Chen, Y. Liu, H. Aryafar, T. Wen, A.S. Lavine, Performance of conical ammonia dissociation reactors for solar thermochemical energy storage, Applied Energy 255 (2019) 113785.
[3] R. Dunn, K. Lovegrove, G. Burgess, A review of ammonia-based thermochemical energy storage for concentrating solar power, Proceedings of the IEEE 100 (2012) 391–400.

[4] C. Zamfirescu, I. Dincer, Hydrogen production from ammonia as an environmentally benign solution for vehicles, Green Energy & Technology 31 (2010) 109–127.
[5] Z.J. Wan, Y.K. Tao, J. Shao, Y.H. Zhang, H.Z. You, Ammonia as an effective hydrogen carrier and a clean fuel for solid oxide fuel cells, Energy Conversion and Management 228 (2021) 113729.
[6] A.E. Karaca, I. Dincer, Ammonia-based energy solutions and research and development efforts in Canada: A perspective, International Journal of Energy Research 44 (2020) 11020–11028.
[7] S. Sasaki, J. Sarlashkar, Internal combustion engine with ammonia fuel, US Patent 8166926 (2012).
[8] A. Valera-Medina, R. Marsh, J. Runyon, D. Pugh, P. Beasley, T. Hughes, P. Bowen, Ammonia-methane combustion in tangential swirl burners for gas turbine power generation, Applied Energy 185 (2017) 1362–1371.
[9] D. Erdemir, I. Dincer, A perspective on the use of ammonia as a clean fuel: Challenges and solutions, International Journal of Energy Research 45 (2021) 4827–4834.
[10] X. Hu, X. Zhu, X. Wu, Y. Cai, X. Tu, Plasma-enhanced NH_3 synthesis over activated carbon-based catalysts: Effect of active metal phase, Plasma Processes and Polymers 17 (2020) e2000072.
[11] Y. Zeng, X. Tu, Plasma-catalytic hydrogenation of CO_2 for the cogeneration of CO and CH_4 in a dielectric barrier discharge reactor: Effect of argon addition, Journal of Physics D: Applied Physics 50 (2017) 184004 (10pp).
[12] M.D. Bai, Z.T. Zhang, X.Y. Bai, M.D. Bai, W. Ning, Plasma synthesis of ammonia with a microgap dielectric barrier discharge at ambient pressure, IEEE Transactions on Plasma Science 31 (2003) 1285–1291.
[13] J.M. Hong, S. Prawer, A.B. Murphy, Production of ammonia by heterogeneous catalysis in a packed-bed dielectric-barrier discharge: Influence of argon addition and voltage, IEEE Transactions on Plasma Science 42 (2014) 2338–2339.
[14] H. Uyama, T. Nakamura, S. Tanaka, O. Matsumoto, Catalytic effect of iron wires on the syntheses of ammonia and hydrazine in a radio-frequency discharge, Plasma Chemistry and Plasma Processing 13 (1993) 117–131.
[15] J. Shah, W. Wang, A. Bogaerts, M.L. Carreon, Ammonia synthesis by radio frequency plasma catalysis: Revealing the underlying mechanisms, ACS Applied Energy Materials 1 (2018) 4824–4839.
[16] K. Sugiyama, K. Akazawa, M. Oshima, H. Miura, O. Nomura, Ammonia synthesis by means of plasma over MgO catalyst, Plasma Chemistry & Plasma Processing 6 (1986) 179–193.
[17] M. Ramakers, I. Michielsen, R. Aerts, V. Meynen, A. Bogaerts, Effect of argon or helium on the CO_2 conversion in a dielectric barrier discharge, Plasma Processes and Polymers 12 (2015) 755–763.
[18] M.S. Moss, K. Yanallah, R.W.K. Allen, F. Pontiga, An investigation of CO_2 splitting using nanosecond pulsed corona discharge: Effect of argon addition on CO_2 conversion and energy efficiency, Plasma Sources Science and Technology 26 (2017) 35009–35027.
[19] H.L. Chen, H.M. Lee, S.H. Chen, T.C. Wei, M.B. Chang, Influence of Ar addition on ozone generation in nonthermal plasmas, Plasma Sources Science and Technology 19 (2010) 65009–65017.
[20] N.V. Kholodkova, I.V. Kholodkov, I.N. Brovikova, The effect of argon addition on the dissociation of oxygen molecules in a DC glow discharge, High Temperature 47 (2009) 448–451.
[21] G.J.M. Hagelaar, L.C. Pitchford, Solving the Boltzmann equation to obtain electron transport coefficients and rate coefficients for fluid models, Plasma Sources Science and Technology 14 (2005)

722–733.
[22] C. Wang, G. Zhang, X. Wang, Comparisons of discharge characteristics of a dielectric barrier discharge with different electrode structures, Vacuum 86 (2012) 960–964.
[23] M. Ben Yaala, D.F. Scherrer, A. Saeedi, L. Moser, K. Soni, R. Steiner, G. De Temmerman, M. Oberkofler, L. Marot, E. Meyer, Plasma-activated catalytic formation of ammonia from N_2-H_2: Influence of temperature and noble gas addition, Nuclear Fusion 60 (2020) 16026–16038.
[24] B.S. Patil, A.S.R. van Kaathoven, F.J.J. Peeters, N. Cherkasov, J.G. Lang, Q. Wang, V. Hessel, Deciphering the synergy between plasma and catalyst support for ammonia synthesis in a packed dielectric barrier discharge reactor, Journal of Physics D: Applied Physics 53 (2020) 144003–144016.
[25] S. Li, T. van Raak, F. Gallucci, Investigating the operation parameters for ammonia synthesis in dielectric barrier discharge reactors, Journal of Physics D: Applied Physics 53 (2020) 14008–14020.
[26] Klaus, Brand, Dielectric strength, boiling point and toxicity of gases - different aspects of the same basic molecular properties, IEEE Transactions on Electrical Insulation 17 (1982) 451–456.
[27] X. Tu, H.J. Gallon, M.V. Twigg, P.A. Gorry, J.C. Whitehead, Dry reforming of methane over a Ni/Al_2O_3 catalyst in a coaxial dielectric barrier discharge reactor, Journal of Physics D: Applied Physics 44 (2011) 274007–274017.
[28] T. Butterworth, R. Elder, R. Allen, Effects of particle size on CO_2 reduction and discharge characteristics in a packed bed plasma reactor, Chemical Engineering Journal 293 (2016) 55–67.
[29] Y. Zhang, J. Li, N. Lu, K. Shang, A. Mizuno, Y. Wu, Evaluation of discharge uniformity and area in surface dielectric barrier discharge at atmospheric pressure, Vacuum 123 (2016) 49–53.
[30] X. Zhu, X. Gao, R. Qin, Y. Zeng, R. Qu, C. Zheng, X. Tu, Plasma-catalytic removal of formaldehyde over Cu-Ce catalysts in a dielectric barrier discharge reactor, Applied Catalysis B: Environmental 170–171 (2015) 293-300.
[31] P. Jamroz, W. Zyrnicki, Optical emission characteristics of glow discharge in the N_2-H_2-$Sn(CH_3)_4$ and N_2-Ar-$Sn(CH_3)_4$ mixtures, Surface and Coating Technology. 201 (2006) 1444–1453.
[32] M. Hannemann, S. Hamann, I. Burlacov, K. Börner, H.J. Spies, J. Röpcke, Langmuir probe and optical diagnostics of active screen N_2-H_2 plasma nitriding processes with admixture of CH_4, Surface and Coating Technology 235 (2013) 561–569.
[33] B.S. Truscott, M.W. Kelly, K.J. Potter, M. Johnson, M.N. Ashfold, Y.A. Mankelevich, Microwave plasma-activated chemical vapor deposition of nitrogen-doped diamond. I. N_2/H_2 and NH_3/H_2 Plasmas, Journal of Physical Chemistry A 119 (2015) 12962–12976.
[34] K.S. Suraj, P. Bharathi, V. Prahlad, S. Mukherjee, Near cathode optical emission spectroscopy in N_2-H_2 glow discharge plasma, Surface and Coating Technology 202 (2007) 301–309.
[35] Y. Wang, M. Craven, X. Yu, J. Ding, P. Bryant, J. Huang, X. Tu, Plasma-enhanced catalytic synthesis of ammonia over a Ni/Al_2O_3 catalyst at near-room temperature: Insights into the importance of the catalyst surface on the reaction mechanism, ACS Catalysis 9 (2019) 10780–10793.
[36] R. Bazinette, J. Paillol, F. Massines, Optical emission spectroscopy of glow, Townsend-like and radiofrequency DBDs in an Ar/NH_3 mixture, Plasma Sources Science and Technology 24 (2015) 55021–55030.
[37] V. Monna, A. Ricard, Emission spectroscopy of Ar-H_2 plasma, Vacuum 61 (2001) 409–412.
[38] R. Miotk, B. Hrycak, M. Jasiński, J. Mizeraczyk, Characterization of an atmospheric-pressure argon plasma generated by 915 MHz microwaves using optical emission spectroscopy, Journal of

Spectroscopy 2017 (2017) 1–6.
[39] A. Gómez-Ramírez, J. Cotrino, R.M. Lambert, A.R. González-Elipe, Efficient synthesis of ammonia from N_2 and H_2 alone in a ferroelectric packed-bed DBD reactor, Plasma Sources Science and Technology 24 (2015) 65011–65018.
[40] J. Hong, S. Pancheshnyi, E. Tam, J.J. Lowke, S. Prawer, A.B. Murphy, Kinetic modelling of NH_3 production in N_2-H_2 non-equilibrium atmospheric-pressure plasma catalysis, Journal of Physics D: Applied Physics 51 (2017) 154005–154038.
[41] R. Aerts, W. Somers, A. Bogaerts, Carbon dioxide splitting in a dielectric barrier discharge plasma: A combined experimental and computational study, ChemSusChem 8 (2015) 702–716.
[42] K. Anzai, H. Kato, M. Hoshino, H. Tanaka, Y. Itikawa, L. Campbell, M.J. Brunger, S.J. Buckman, H. Cho, F. Blanco, Cross section data sets for electron collisions with H_2, O_2, CO, CO_2, N_2O and H_2O, European Physical Journal D 66 (2012) 36.
[43] X. Zhu, X. Hu, X. Wu, Y. Cai, H. Zhang, X. Tu, Ammonia synthesis over γ-Al_2O_3 pellets in a packed-bed dielectric barrier discharge reactor, Journal of Physics D: Applied Physics 53 (2020) 164002 (8pp).
[44] V. Guerra, E. Tatarova, C.M. Ferreira, Kinetics of metastable atoms and molecules in N_2 microwave discharges, Vacuum 69 (2002) 171–176.
[45] J.F.D.L. Fuente, S.H. Moreno, A.I. Stankiewicz, G.D. Stefanidis, A new methodology for the reduction of vibrational kinetics in non-equilibrium microwave plasma: Application to CO_2 dissociation, Reaction Chemistry & Engineering 1 (2016) 540–554.
[46] M. Sode, W. Jacob, T. Schwarz-Selinger, H. Kersten, Measurement and modeling of neutral, radical, and ion densities in H_2-N_2-Ar plasmas, Journal of Applied Physics 117 (2015) 083303 (19pp).
[47] J. Nakajima, H. Sekiguchi, Synthesis of ammonia using microwave discharge at atmospheric pressure, Thin Solid Films 516 (2008) 4446–4451.
[48] A. Qayyum, S. Zeb, M.A. Naveed, N.U. Rehman, S.A. Ghauri, M. Zakaullah, Optical emission spectroscopy of Ar-N_2 mixture plasma, Journal of Quantitative Spectroscopy and Radiative Transfer 107 (2007) 361–371.
[49] J. Hong, S. Prawer, A.B. Murphy, Plasma catalysis as an alternative route for ammonia production: status, mechanisms, and prospects for progress, Acs Sustainable Chemistry & Engineering 6 (2018) 15–31.